

Testing Two Predictions for Fracture Load Using Computer Models of Trabecular Bone

Michael A. K. Liebschner,* Ralph Müller,[†] Sunil J. Wimalawansa,[‡] Chamith S. Rajapakse,[§] and Gemunu H. Gunaratne^{§¶}

*Department of Bioengineering, Rice University, Houston, Texas; [†]Institute for Biomedical Engineering, Swiss Federal Institute of Technology and University of Zürich, Zürich, Switzerland; [‡]Department of Medicine, Robert Wood Johnson Medical School, New Brunswick, New Jersey; [§]Department of Physics, University of Houston, Houston, Texas; and [¶]The Institute of Fundamental Studies, Kandy, Sri Lanka

ABSTRACT Aging induces several types of architectural changes in trabecular bone including thinning, increased levels of anisotropy, and perforation. It has been determined, on the basis of analysis of mathematical models, that reduction in fracture load caused by perforation is significantly higher than those due to equivalent levels of thinning or anisotropy. The analysis has also provided an expression which relates the fractional reduction of strength τ to the fraction of elements ν that have been removed from a network. Further, it was proposed that the ratio Γ of the elastic constant of a sample and its linear response at resonance can be used as a surrogate for τ . Experimental validation of these predictions requires following architectural changes in a given sample of trabecular bone; techniques to study such changes using microcomputed tomography are only beginning to be available. In the present study, we use anatomically accurate computer models constructed from digitized images of bone samples for the purpose. Images of healthy bone are subjected to successive levels of synthetic degradation via surface erosion. Computer models constructed from these images are used to calculate their fracture load and other mechanical properties. Results from these computations are shown to be consistent with predictions derived from the analysis of mathematical models. Although the form of $\tau(\nu)$ is known, parameters in the expression are expected to be sample-specific, and hence ν is not a reliable predictor of strength. We provide an example to demonstrate this. In contrast, analysis of model networks shows that the linear part of $\tau(\Gamma)$ depends only on the structure of trabecular bone. Computations on models constructed from samples of iliac crest trabecular bone are shown to be in agreement with this assertion. Since Γ can be computed from a vibrational assessment of bone, we argue that the latter can be used to introduce new surrogates for bone strength and hence diagnostic tools for osteoporosis.

INTRODUCTION

The fracture load of trabecular bone, which is a critical component of bone strength, depends on many factors. They include architectural characteristics such as the levels of connectivity, perforation, thinning, and anisotropy, as well as subarchitectural properties of bone like the mineral content (1,2) and the density of diffuse damage (3–8). To develop reliable surrogates for fracture load, it is necessary to first determine those factors most critical to strength, and whose changes are thus most damaging. The next step is to identify (preferably) noninvasive measurements that can be used to estimate age-related changes in these critical factors. The problem with implementing such a program on bone is the inability to control variations in individual characteristics; for example, no protocols are known that increase the level of perforation in animal trabecular bone while keeping all remaining factors unchanged. An alternative method to address the issue is to conduct initial studies in suitable mathematical models.

Silva and co-workers (9–11) and Guo and Kim (12) introduced and analyzed one such mathematical model. It consists of random networks constructed using the Voronoi algorithm. In these Voronoi networks, trabecular elements

are represented by freely pivoted elastic struts; on average, there are between three and four struts meeting at a node. An externally applied deformation changes locations of nodes and lengths of struts, thus allowing for storage of elastic energy. Computational analysis of such networks was used to infer that, among known age-related changes of bone, trabecular perforation is the most damaging in the sense that, for a given reduction in mass, it leads to the most significant loss of fracture load. In particular, uniform thinning of trabecular elements and increases in anisotropy were shown to play a secondary role (9,12).

The significance of trabecular removal in reducing fracture load leads to an interesting observation. It is known from percolation theory (13) that when a fraction ν_0 of struts are randomly removed from a large network, it will spontaneously fragment into multiple segments; in particular, its strength will vanish at this point. The value of ν_0 , known as the *bond-percolation threshold*, depends on the class of networks; for three-dimensional Voronoi structures its value is $\nu_0 = 0.5$. Thus, when half the struts on a Voronoi network are randomly removed, its fracture load vanishes. Since trabecular perforation has been shown to be the dominant cause of loss of bone strength, it can be expected that the fracture load of trabecular bone will vanish whereas its mass is non-zero. Consequently, the commonly used power-law relationship between fracture load and density of bone

Submitted December 3, 2004, and accepted for publication April 8, 2005.

Address reprint requests to Gemunu H. Gunaratne, E-mail: gemunu@uh.edu.

© 2005 by the Biophysical Society

0006-3495/05/08/759/09 \$2.00

doi: 10.1529/biophysj.104.057539

(14–18) can only be an approximation that is invalid for weak bones; for, under a power-law, both the strength (i.e., fracture load) and density will vanish simultaneously.

Clearly, analysis of mathematical models can provide useful information regarding bone strength. There is, however, one modification needed in the model—namely to correctly account for the fact that local structure of trabecular bone resembles disordered cubic networks more closely than Voronoi networks (19,20). The mean number of struts joined at a node, and hence the percolation threshold ν_0 , for the two classes of networks is different. For cubic networks, $\nu_0 \approx 0.7508$; i.e., approximately three-quarters of the struts need to be removed before spontaneous fragmentation (13). Consequently, loss of strength of a trabecular bone sample may be expected to be slower than for Voronoi networks. We have conducted an analysis of a disordered cubic struts-and-nodes model with bond-bending energies (21). It was shown, as in the case for Voronoi networks (9,11), that the segment of bone most active in load transmission (referred to as the *stress backbone*) experiences occasional dramatic changes as trabecular elements are removed. The cause of such changes was shown to be the formation of long fractures (22), which prevent many struts in the neighborhood (for example, those immediately above and below the fracture) from taking part in transmission of an externally applied load. In fact, as struts continue to be removed, the stress backbone becomes extremely sparse, consisting of a handful of pathways lying (roughly) along the loading direction. This inefficiency continues to be the principal cause of reduction of fracture load even when factors like trabecular thinning and anisotropy are included in the model (23).

We have previously introduced expressions that relate reductions in the fracture load to 1), the fraction of elements removed from a network (21); and 2), a ratio of response functions of a network (22) (see Theoretical Considerations, below). The aim of the work reported here is to test the validity of these expressions using anatomically accurate computer models.

In this article, we only consider architectural changes of a trabecular bone specimen. Consequences of variations in material properties of bone tissue (1,2), and complex interactions between the two facets of bone are not analyzed. For example, the specimen may be weaker than predicted by our computations if critical load-carrying segments have weaker biomechanical properties. However, analysis of mathematical models show that Eqs. 1 and 2 are valid even when such variations are included (22,21).

THEORETICAL CONSIDERATIONS

Reduction of fracture load with density

Analysis of mathematical models can be used to deduce an expression that represents reductions in fracture load caused by the random removal of a fraction ν of trabecular elements

(21). There are three ingredients needed for the derivation. The first is a computation of the loss of strength due to a single penny-shaped fracture of circular cross-section and height l . The stresses on struts bordering the fracture increase with the diameter (21,24). Consequently, these elements have a higher propensity for fracture, thus weakening the entire network. This argument shows, in addition, that the size of the largest fracture(s) determines the strength of a network (25). The second ingredient needed for the derivation is an estimate of the size of the largest fracture. This can be obtained by probabilistic considerations (21). The final piece of information needed is the symbiotic effects between multiple fractures. Although such a calculation is extremely difficult, general results from percolation theory can be used to deduce how the expressions derived thus far need to be modified (21). The expression for the maximum stress $\sigma_{\max}(\nu)$ suggested by the analysis is

$$\tau(\nu) \equiv \frac{\sigma_{\max}(\nu)}{\sigma_{\max}(0)} = \frac{1}{1 + a_1 z^{-\psi/2} + a_2 z^{-\psi}}, \quad (1)$$

where $\sigma_{\max}(0)$ is the peak strength (i.e., the fracture strain for an undamaged network where $\nu = 0$). The variable $z \equiv \log(\nu_0/\nu)$, and a_1 , a_2 , and ψ depend on the model parameters and the number of nodes in the network. In particular, they depend on the level of trabecular thinning and the relative strength of bond-bending (compared to elastic) terms (21).

Loss of strength and linear response

The second assertion to be tested involves a surrogate for bone strength that is obtained from the response of a sample of trabecular bone to externally applied strain. The basic idea, as alluded to before, is that the inefficiency of load transmission is the principal cause for reduction of fracture load. We suggest that the reduction in bone strength can be estimated by *the fraction of struts belonging to the stress backbone*. It can be obtained if the number of trabeculae that belong to the stress backbone and the total number of elements on a sample are known. The following observations provide a method to estimate these quantities. First, the elastic modulus $\chi(0)$ of a sample depends on the number of stress pathways, because each such pathway allows additional load to be transmitted. The second observation is that the response $\chi(\Omega)$ of the sample to sonic or ultrasonic vibrations of a sufficiently high frequency Ω can be used to estimate the number of struts on the network. Under these conditions, signals are attenuated very quickly inside the sample, and stresses are limited to the immediate neighborhood of the surface that is driven. As a result, the presence of large fractures in the interior of the network, which reduce the extent of the stress backbone, play no role in the response to high-frequency driving; i.e., all trabecular elements near the surface contribute to $\chi(\Omega)$. In computations reported here, we take Ω to be the resonance frequency of the sample.

Thus, the ratio $\Gamma \equiv \chi(0)/\chi(\Omega)$, which can be obtained from vibrational analysis, provides an estimate for the reduction in fracture load. The relationship was shown to take the form (22)

$$\tau = A\Gamma + h(\Gamma), \quad (2)$$

where $h(\Gamma)$ represents higher order nonlinear terms which are model-dependent and are insignificant when Γ is small. According to Eq. 2, when the fracture load of a bone is much smaller than its peak value (i.e., in the case which is relevant in the search for osteoporotic damage), τ is proportional to Γ and $\tau(\Gamma)$ passes through the origin. These are important features for Γ to be useful as a surrogate for bone strength.

It should be noted that response functions can be obtained from a vibrational assessment of a bone sample. The value Ω is the driving frequency at which the response is maximized. The value $\chi(0)$ can be obtained by extrapolating the curve $\chi(\omega)$ to $\omega = 0$ (i.e., the low-frequency limit).

Thus τ can be estimated using measurements that can conceivably be made in vivo by application of sonic or ultrasonic vibrations. As has been argued earlier (20), we expect τ to be more relevant than the fracture load σ_{\max} in identifying patients suffering from osteoporosis. The underlying reason is that it is easy to imagine a scenario where the fracture load of a osteoporotic heavy subject is larger than that of a healthy normal subject (20). Furthermore, analysis of mathematical models (26,22) has shown that τ is more robust to variations in the system parameters than σ_{\max} .

METHODS

Micro-CT imaging

The imaging techniques are described in detail elsewhere (27,28). The vertebral and iliac crest samples were scanned with a high-resolution micro-CT system $\mu CT 20$ (Scanco Medical, Bassersdorf, Switzerland). Cubic voxels with sides $14 \mu m$ were used to represent the trabecular bone samples. The bone biopsies were placed in an airtight cylindrical sample holder filled with formaldehyde; no further sample preparation was necessary. The images used in the study were obtained from cubic sections whose sides were ~ 3.5 mm. The grayscale images were segmented using a low-pass filter to remove noise and a fixed threshold to extract the mineralized bone phase.

The analysis described below is conducted on one sample each of vertebral and iliac crest trabecular bone. Each sample is represented by occupancy in a $256 \times 256 \times 256$ lattice.

Lattice spring models

Computations reported in this article are conducted on lattice spring models constructed from digitized images of trabecular bone samples (29,30). Each occupied voxel of the image is replaced by a set of linear elastic elements as described below. The choice of springs and their elastic moduli are set by the following requirement: a spring network which is constructed to represent an isotropic region should itself be isotropic (30). Although it is known that no cubic-type network can satisfy this condition exactly (31), the following combination was shown to provide a stable and approximately isotropic configuration of elastic elements. Each occupied voxel is replaced by a set of 24 elements; 12 of these with identical elastic constant k lie along the sides of

the cube, whereas the remaining 12, with elastic moduli $2k$ are placed along the face-diagonals (29,30). The lattice spring model representing the sample of trabecular bone is the network constructed by replacing each occupied voxel of the digitized image by such a combination of springs.

We study the behavior of the lattice spring network under compression in the axial (vertical) direction. The boundary conditions imposed on the network are as follows: Nodes on the lower surface are free to move horizontally, but their vertical positions remain fixed. Those on the upper surface are subjected to a vertical compression ζ , and are free to move horizontally. All remaining nodes are constrained only by springs connecting them to neighbors. The elastic potential energy of the compressed network can be calculated from the coordinates of the nodes, which are the independent variables in the system. Equilibrium of the network subjected to a compression ζ is calculated by minimizing its elastic energy using the conjugate gradient method (32).

As the external compression ζ is increased the most highly stressed locations become susceptible to fracture. There have been theoretical studies of fracture in composite material such as bone (1,2). However, to the best of our knowledge, there have not been reports of experimental studies on fracture of trabecular bone tissue. On the other hand, several recent experiments have demonstrated that fracture strains for specimens of human trabecular bone of a fixed size from specific anatomical locations are nearly constant for a wide range in age, even though the corresponding fracture load can vary by more than an order of magnitude (33–39).

These experimental findings motivate us to model failure of bone tissue with a strain-based criterion. We model failure of individual voxels; specifically, at each value of ζ , voxels which are strained beyond a preset value η are removed from the model network. The amount of strain used in these considerations is the largest eigenvalue of the strain tensor (29); thus, the failure of a voxel is associated with it being strained beyond η along *any* one direction. Under this scenario, we find that failure strains of lattice spring networks remain nearly fixed during degradation. It should be noted that the fracture strain of a specimen is expected to reduce with increasing size due to the likelihood of larger fractures (1,25,20).

The lattice spring system needs to be extended to model dynamical properties of bone samples. We replace the mass m of material contained within each voxel by identical point masses $1/8 m$ placed on each of its eight vertices. Thus, we model mechanical properties of the bone specimen by a network of elastic elements with masses placed on the nodes. The mass m_i at node i is $n'_i m/8$, where $n'_i \leq 8$ is the number of occupied voxels surrounding it. Similarly, the elastic modulus $k g_{ij}$ joining nodes i and j depends on the number of occupied voxels with ij as an edge. The Hamiltonian of the network is (30)

$$H = \sum_i \frac{\mathbf{p}_i^2}{2m_i} + \frac{1}{4} k \sum_{ij} g_{ij} [(\mathbf{u}_i - \mathbf{u}_j) \cdot \hat{\mathbf{x}}_{ij}]^2, \quad (3)$$

where \mathbf{p}_i denotes the momentum of the mass at node i and \mathbf{u}_i denotes its displacement. The value $\hat{\mathbf{x}}_{ij}$ denotes the unit vector in the direction from node i to node j .

The damping caused by surrounding soft tissue during the motion of a trabecular network is represented by a linear dissipation $-\gamma \mathbf{v}$ on each mass. Here \mathbf{v} is the velocity of the node and the damping coefficient γ is a model parameter. Note that although $\sigma_{\max}(\nu)$ and $\sigma_{\max}(0)$ depend on the values of the parameters k and η , the ratio τ is independent of them. Further, computations of model systems show that Γ is only weakly dependent on m and γ . Thus, it is not necessary to know these mechanical parameters of bone tissue to test the validity of Eqs. 1 and 2.

To accelerate computations, we reduce the size of the lattice spring model by forming units of $b \times b \times b$ voxels for the analysis. A unit with a fraction f occupied voxels (i.e., the grayscale on a coarse-grained structure) is replaced by one of uniform density whose mass and elastic constants are reduced by a factor f . Note that although the model is homogenized at the level of units, it is inhomogeneous on a larger scale. Similar inhomogeneous models have been shown to improve predictions on mechanical properties of trabecular bone (40).

The elastic modulus $\chi(0)$ is the slope of the stress-versus-strain curve at the yield point. The value σ_{\max} is calculated from the stress-versus-strain curve obtained using incremental increases of the external deformation. Voxels strained beyond η are removed at each stage and equilibrium is recalculated. The maximum of the stress versus strain curve is chosen to be σ_{\max} . Note that, even though the voxels are taken to be brittle, our computations show that a trabecular sample is highly plastic; typically peak load is reached at a strain which is approximately an order-of-magnitude larger than the yield strain, and the network remain strong even beyond. This is possible because, following a fracture of a voxel, the network is able to find alternative stress pathways to transmit an external load.

In this article, we model disuse osteoporosis (e.g., during bed-rest or extended space travel) by synthetically degrading a bone sample by uniform resorption of material from its surface (41,12). This process imposes trabecular thinning as well as changes in the levels of anisotropy and perforation of trabecular bone. Specifically, all voxels that have nine or fewer occupied neighbors are removed at each level of surface erosion; i.e., any voxel that sticks out of a surface or lies on an edge of the sample is eliminated at the next level. The vertebral bone sample can be subjected to seven such erosions before it fragments, whereas the iliac crest sample (with thicker trabeculae) fragments following 11 levels of erosion. Note that surface erosion of the samples is implemented before blocking of voxels into larger units. It should be noted that age-related osteoporosis is more appropriately modeled by a different mechanism (42), and tests of Eqs. 1 and 2 under such a scenario can be studied. Analysis of mathematical models indicates that the two expressions will be valid under such distinct modes of degradation (21,23).

The analysis of bone samples was conducted using blocks of side $b = 4$ and hence each side of the cubic unit was $56 \mu\text{m}$. The network so constructed contained $64 \times 64 \times 64$ units. We have also conducted a few computer experiments with higher resolution ($28 \mu\text{m}$) to confirm that our conclusions remain unchanged. Models at this resolution have been shown to give accurate values for mechanical parameters of a bone sample (43,44).

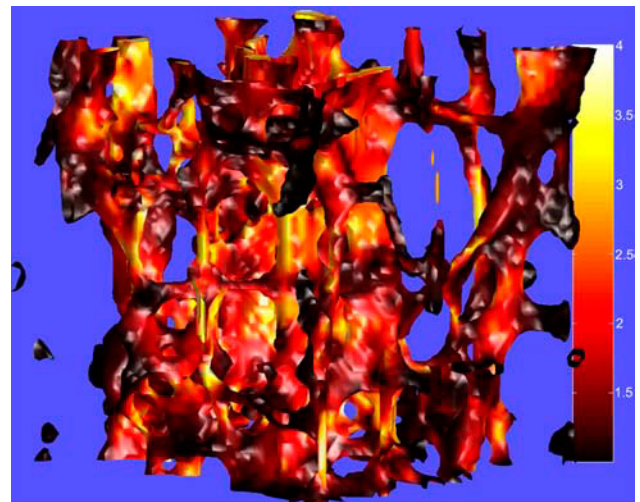
Data analysis

Trabecular bone samples used in our study were harvested from young subjects. It is assumed that these samples contained very few perforations. This assertion was confirmed by visual inspection of the images (see Fig. 1 *a*), and $\sigma_{\max}(0)$ was chosen to be the fracture strain of this computer model. The peak density $\rho(0)$ was estimated by the fraction of occupied voxels in the digitized image. Each level of surface erosion removes voxels from a network, and consequently reduces the density and fracture load. Their values following n -levels of erosion are denoted by $\rho(n)$ and $\sigma_{\max}(n)$, respectively. The fraction $\nu(n)$ is estimated by comparing the density of the sample with $\rho(0)$ via

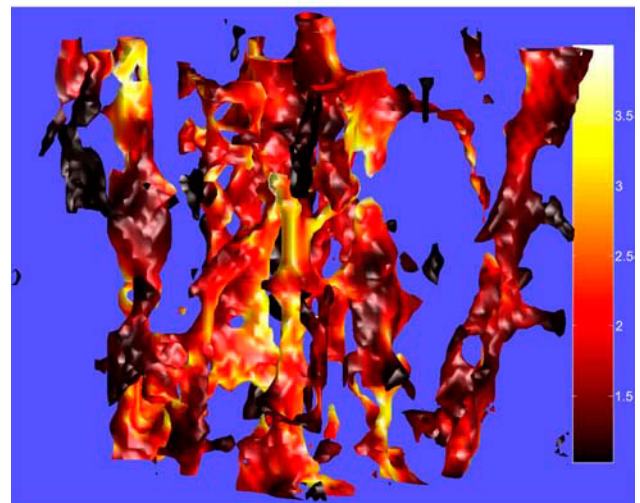
$$1 - \nu(n) = \frac{\rho(n)}{\rho(0)}. \quad (4)$$

This expression is strictly valid if the only change in bone architecture is trabecular removal. However, analysis of mathematical models have shown that Eq. 1 is valid with this assignment even in cases where complementary causes of bone damage such as trabecular thinning and anisotropy are included (21,23). We believe that the underlying reason is that reductions in strength caused by trabecular perforations dominate changes due to other causes. Note that, since ν does not appear in Eq. 2, the assignment in Eq. 4 is not required to test its validity.

Once the values of $\nu(n)$ and $\tau(n)$ are available, parameters a_1 , a_2 , and ψ of Eq. 1 are obtained using a nonlinear least-square data fitting using the Gauss-Newton method (32). The routine *nlinfit* from MATLAB (The MathWorks, Cambridge, UK) is used for the purpose. Error estimates provided correspond to a 95% confidence level. The root-mean square values for each fit is given. A corresponding analysis was used to test the validity of Eq. 2.



(a)



(b)

FIGURE 1 The strain on cubic units of voxels in uniformly compressed computer models constructed (a) from the original vertebral trabecular bone, and (b) one obtained following six levels of surface erosion. Each network is compressed uniformly by an amount $\zeta = 0.1$, where the unit of length is defined to be the side of a block containing $4 \times 4 \times 4$ voxels, i.e., $56 \mu\text{m}$. In these figures, dark red denotes the smallest values of the strain whereas bright yellow denotes the highest values. Observe that the locations under high strain form a few vertical pathways in the second case.

RESULTS

Changes in the stress distribution

The image of vertebral bone can be degraded seven times via surface erosion before fragmentation. If it is assumed that the density of bone tissue is uniform within the specimen, then the bone mineral density is proportional to the fraction of voxels (of the 256^3 volume elements) that are occupied. The porosity (i.e., $1 - \text{fraction of occupied voxels}$) at each level of erosion is given in column 2 of Table 1. The elastic modulus k was set to four units.

TABLE 1 Mechanical properties of the computer model constructed from the digitized image of the specimen of vertebral bone and those obtained from seven successive levels of surface erosion; the units associated with each variable are defined in the text

Level	Porosity	Fracture load	$\chi(\Omega)$	$\chi(0)$
0	86.3%	6.85×10^1	1.15×10^4	33.97
1	88.0%	5.65×10^1	1.00×10^4	27.29
2	89.7%	3.93×10^1	8.66×10^3	20.67
3	91.2%	2.97×10^1	7.36×10^3	13.43
4	92.7%	1.53×10^1	6.13×10^3	5.86
5	94.7%	5.66	4.93×10^3	2.32
6	95.3%	3.08	3.85×10^3	8.16×10^{-1}
7	96.3%	1.46	2.87×10^2	1.83×10^{-2}

To calculate the stress distribution on model networks, we compress each by a fixed uniform strain of $\zeta = 0.1$ units along the principal axis; at this compression none of the voxels are fractured. Fig. 1, *a* and *b*, shows strain distributions on the original network I_0 and another, I_6 , constructed following six levels of surface erosion. Unlike in Fig. 1 *a*, units experiencing large strain (shown in yellow or white) in Fig. 1 *b* are organized along a few vertical pathways. Fig. 2 shows the histogram of strains on the blocks of voxels for the two cases. It is seen that a significantly larger fraction of voxels in I_6 experience very small levels of strain, and are not active in load transmission. Most units whose strain lies in the tail of the histogram belong to the stress backbone.

Similar observations are made on changes in the stress backbone that accompany erosion of the iliac crest sample. The computer model can be degraded 11 times before fragmentation. The porosity at successive levels of erosion is given in column 2 of Table 2.

Relationship between fracture load and density

The strain-based fracture criterion imposed on individual blocks of voxels was defined by $\eta = 10\%$; i.e., any unit whose strain tensor has an eigenvalue larger than 0.1 is removed from the network. (Note that conclusions reported in this article are independent of η . This assertion was verified computationally.) The values of $\sigma_{\max}(n)$ for synthetically degraded vertebral and iliac crest samples are given in the third columns of Tables 1 and 2, respectively.

Fig. 3, *a* and *b*, show relationships between reduction in fracture load and the fraction of occupied voxels for the two groups of model networks. In each case the networks are seen to fragment (i.e., σ_{\max} vanishes) when roughly three-quarters of the original voxels are removed. This is consistent with the value $\nu_0 \approx 0.75$ for the percolation threshold of cubic networks.

Dashed lines in each figure show the best fit to Eq. 1, confirming that it provides a good representation of the

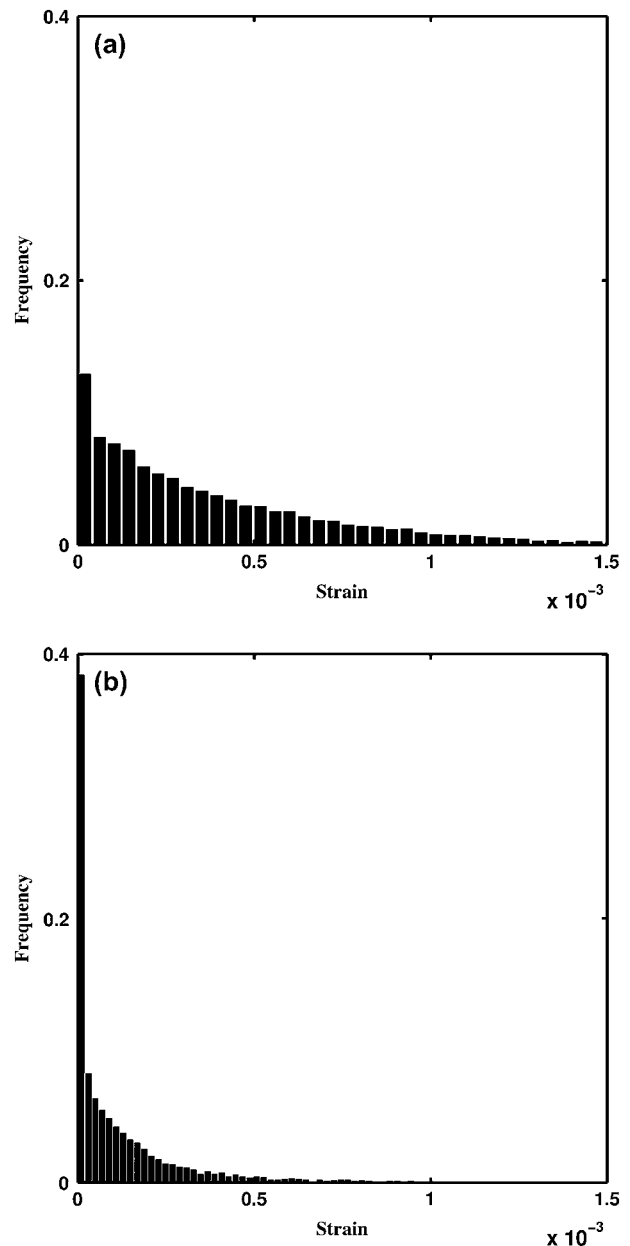


FIGURE 2 Histograms of stress distributions for the compressed networks shown in Fig. 6. The kurtosis eq_6 is 2.15 for the original network and is 17.4 for the degraded one, showing that the latter has a significantly broader tail.

reduction in fracture load in a bone sample due to surface erosion. The parameters for the fit in Fig. 3 *a* are $a_1 = -0.391 \pm 1.075$, $a_2 = 1.198 \pm 1.188$, and $\psi = 1.618 \pm 0.805$, whereas those for the fit in Fig. 3 *b* are $a_1 = -0.858 \pm 0.517$, $a_2 = 1.738 \pm 0.576$, and $\psi = 1.354 \pm 0.282$. The root-mean-square values for the two fits are 0.020 and 0.016, respectively. Note that, when the only source of damage is trabecular perforation and the network is large, the value of ψ is the universal index 1.8 for three-dimensional percolation networks (45). However, ψ can be different for small

TABLE 2 Mechanical properties of the computer model constructed from the digitized image of the specimen of iliac crest bone and those obtained from 11 successive levels of surface erosion; the units associated with each variable are defined in the text

Level	Porosity	Fracture load	$\chi(\Omega)$	$\chi(0)$
0	71.8%	8.10×10^1	2.24×10^4	37.96
1	74.3%	7.20×10^1	2.18×10^4	31.01
2	76.6%	6.20×10^1	2.03×10^4	25.18
3	78.8%	4.78×10^1	1.88×10^4	19.99
4	80.9%	3.55×10^1	1.74×10^4	15.17
5	83.0%	2.40×10^1	1.59×10^4	10.81
6	84.9%	2.02×10^1	1.46×10^4	7.48
7	86.7%	1.25×10^1	1.32×10^4	5.02
8	88.4%	8.20	1.19×10^4	3.15
9	89.9%	5.28	1.07×10^4	1.91
10	91.3%	2.47	9.52×10^3	1.01
11	92.5%	1.38	8.43×10^3	0.48

networks and for those where other architectural factors of bone damage are included (21).

Relationship between fracture load and vibrational response

In testing the validity of Eq. 2, m and γ were set to 0.005 and 0.1, respectively. The function $\chi(\omega)$ was evaluated for a range of driving frequencies ω , and the location of its peak was chosen to be the resonance frequency Ω . Fig. 4 shows the strain distributions on the networks of Fig. 1 at resonance with driving amplitude of 0.01 units. Notice that, unlike for application of a stationary external strain, the entire top layer of trabecular elements experiences nearly uniform compression at all levels of surface erosion, as can be seen by comparing the top layers of Figs. 1 *b* and 4 *b*. The value $\chi(0)$ can also be obtained from the low frequency limit of $\chi(\omega)$.

Values of the responses $\chi(\Omega)$ and $\chi(0)$ of synthetically degraded models of vertebral and iliac crest samples are given in columns 4 and 5 of Tables 1 and 2. The relationship between $\tau(n)$ and $\Gamma(n)$ for the samples are shown in Fig. 5, *a* and *b*, respectively. The results appear to extrapolate to the origin as predicted (22). A nonlinear function $h(\Gamma) = B\Gamma^2$ gives the dashed line in Fig. 5 *b*, and the fit is obtained for $10^{-2}A = 4.12 \pm 0.95$ and $10^{-4}B = 12.52 \pm 7.08$. For the vertebral bone a significantly better fit is obtained using $h(\Gamma) = B\Gamma^\beta$, with parameters $10^{-2}A = 0.59 \pm 0.90$, $10^{-4}B = 66.7 \pm 194.0$, and $\beta = 4.27 \pm 2.92$. the root-mean square values for the iliac crest and vertebral samples were 0.033 and 0.042, respectively.

DISCUSSION

The purpose of the work reported in this article was to test several conclusions that were made on the basis of an analysis of a mathematical model of trabecular bone (26). One assertion is that changes in the stress-carrying backbone

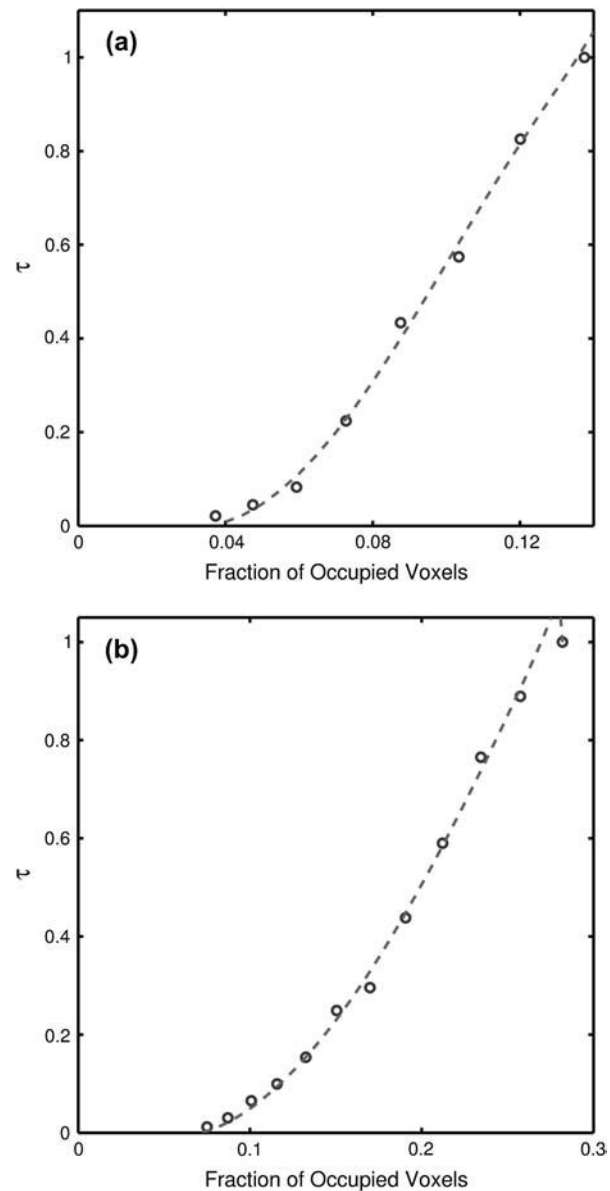


FIGURE 3 The relationship between loss of fracture load τ and the fraction of occupied voxels for the models of trabecular bone from the (a) vertebra, and (b) iliac crest subjected to architectural degradation through surface erosion. Assuming a uniform density of bone tissue, Eq. 4 can be used to estimate ν from the fraction of occupied voxels. Eq. 1 can then be used to evaluate τ . The dashed lines represent the best fit.

due to trabecular perforation plays a dominant role in reductions of bone strength. Analysis based on this observation provides the relationships in Eqs. 1 and 2 for reduction of fracture load. In the former, τ is related to reductions in the density ρ of a sample of trabecular bone from its peak value $\rho(0)$. In the latter, τ is related to a ratio Γ of the elastic modulus of the sample and its response at resonance. Experimentally, these response functions can be obtained by subjecting the sample to sonic or ultrasonic vibrations; resonance is identified from the peak of $\chi(\omega)$, and $\chi(0)$ is its

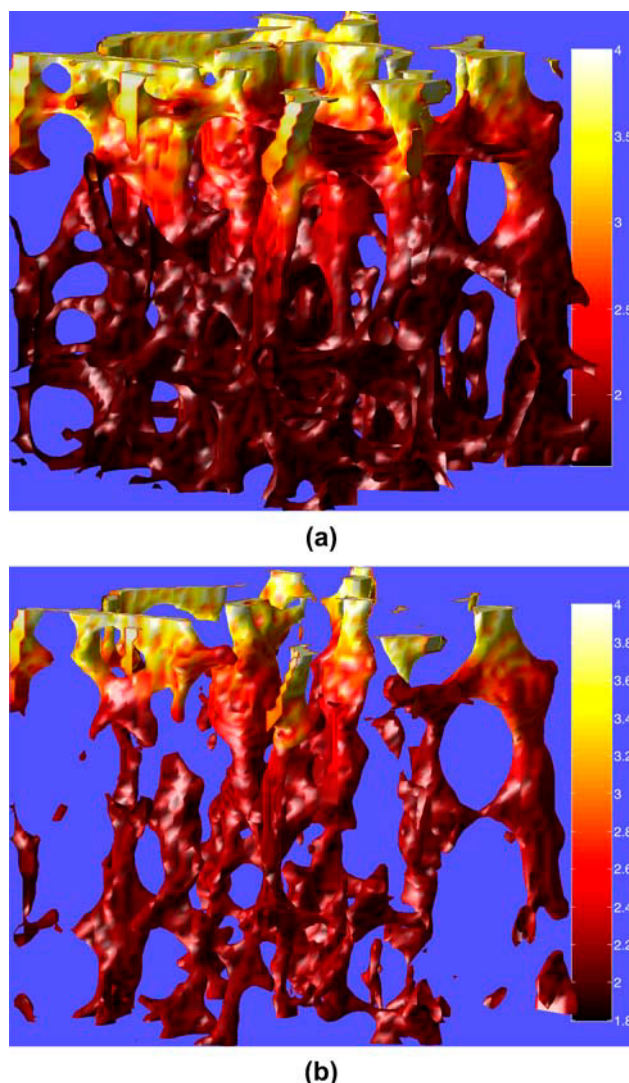


FIGURE 4 The distribution of strain on models shown in Fig. 6 at resonant driving. Only trabecular elements near the externally driven surface experience significant compression and all such elements are compressed by nearly the same amount.

low-frequency limit. Consequently, it is conceivable that a noninvasive diagnostic tool for bone strength be developed based on vibrational assessment.

As we have argued, testing the expressions in Eqs. 1 and 2 require following the degradation of a *given sample of trabecular bone*. In work reported here, we have conducted computational studies on anatomically accurate models constructed using digitized images of bone. These models were subjected to successive levels of synthetic degradation by erosion of voxels.

Analysis of mathematical models indicates that reductions in bone strength are caused primarily by the inability of a weak bone to effectively use the remaining segments for stress transmission (21,23). As seen from Fig. 1, such reductions in the extent of the stress backbone appear to be a

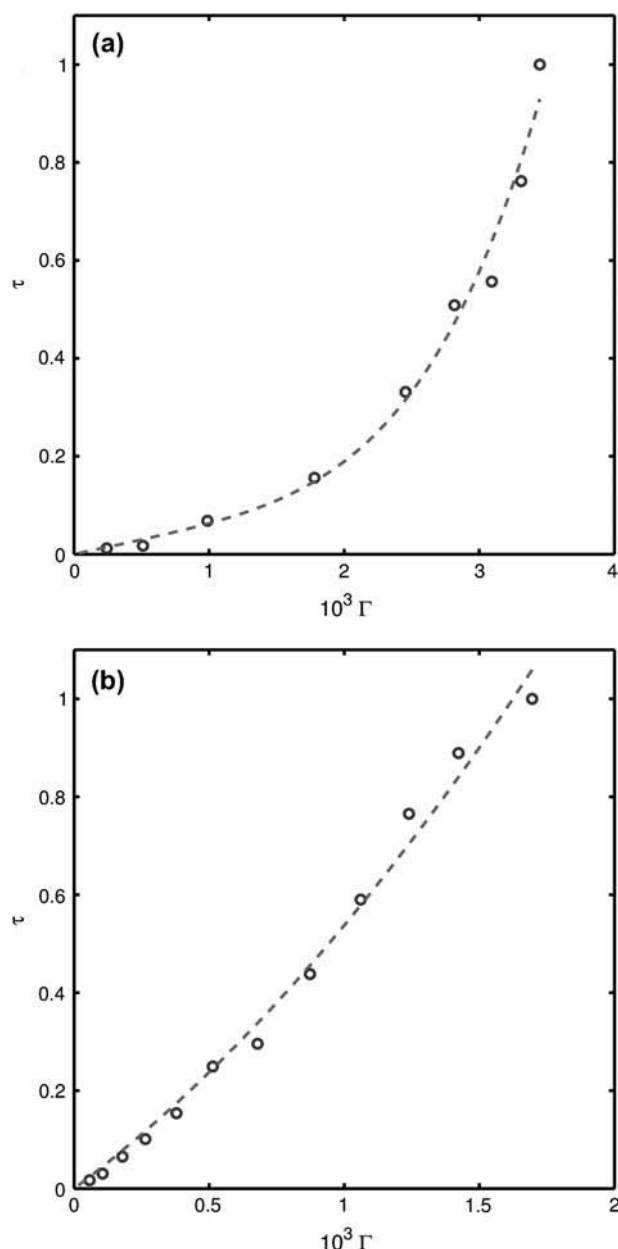


FIGURE 5 The relationship between Γ and τ for bone samples subjected to surface erosion. Results for the sample of vertebral bone are shown in *a*, whereas those for the sample of iliac crest bone are shown in *b*. The dashed lines represent the best fit to Eq. 2.

feature of the computer models as well. Unfortunately, experimental methods to test this assertion in vivo are currently not available.

Since the extent of the stress backbone plays such a significant role in determining the fracture load, bone density is unlikely to be a reliable surrogate for fracture load. How can this conclusion be reconciled with the exceptionally good agreement shown in Fig. 3, *a* and *b*? It is important to recognize that the parameters a_1 , a_2 , and ψ in Eq. 1 depend on the type of damage incurred by a bone sample. For example,

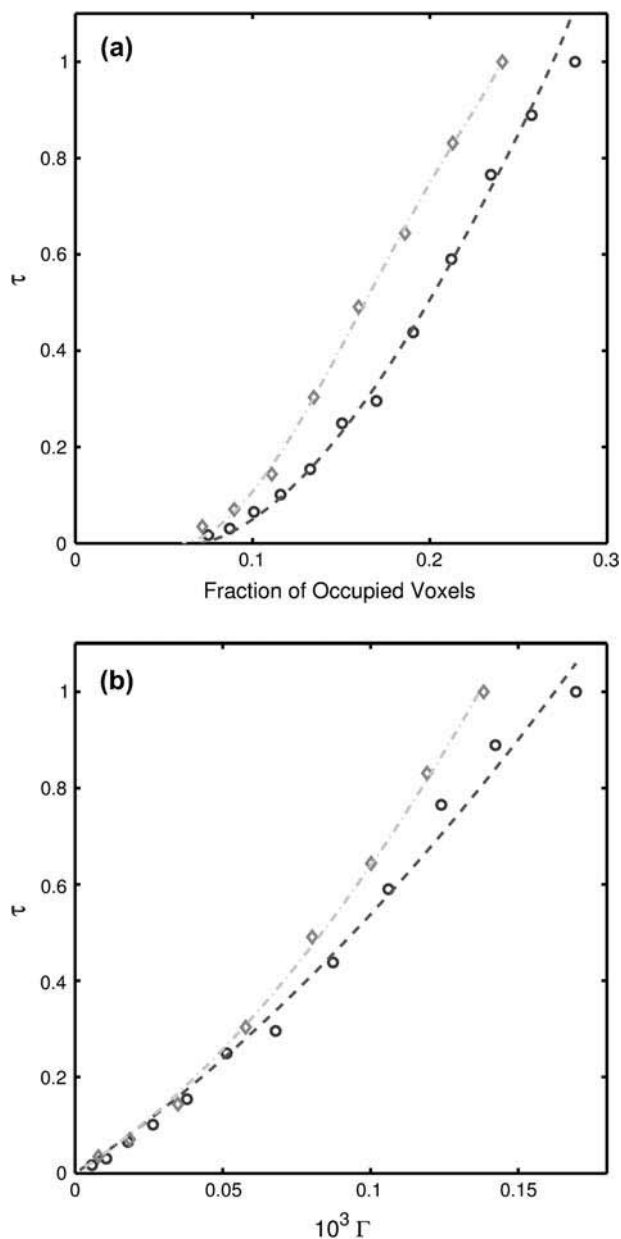


FIGURE 6 The curves relating (a) τ to the fraction of occupied voxels, and (b) τ to Γ for two samples of trabecular bone from the iliac crest.

they depend on the levels of trabecular thinning and anisotropy (23). Thus, although $\tau = 1$ for the undamaged sample and τ vanishes when nearly 75% of the mass is removed, its values for intermediate densities depend on the values of a_1 , a_2 , and ψ . In other words, it is conceivable that there are significant variations in $\tau(\nu)$ between samples, related to differences in the nature of bone damage. Fig. 6a shows results from the analysis of two samples of trabecular bone from the iliac crest. Clearly, there are significant differences between τ for a given occupancy (or density), consistent with many previous studies (46,33); hence it will be difficult to estimate the strength of the sample from the density.

In contrast, the linear part of Eq. 2 depends only on generic factors like the type of the network (cubic, Voronoi, platelike) (22), and it is not expected to differ between multiple samples from a fixed anatomical location. If confirmed, it will lend further credence to the assertion that vibrational assessment could be the basis of reliable diagnostics for fracture load of trabecular bone. Fig. 6b shows $\tau(\Gamma)$ for the same two samples of trabecular bone from the iliac crest. It is clear that they converge to a common line when Γ is small (i.e., the limit where reliable diagnostics are most needed). However, it should be noted that an analysis of a much larger group of trabecular samples (as well as analysis of samples from other anatomical locations) would be needed to make definitive conclusions about the specimen independence of $\tau(\Gamma)$.

One issue remains to be resolved. It should be noted that evaluating the response of trabecular bone in vivo is a nontrivial task. As an example, suppose we were to subject the vertebrae for such an analysis. The best we can do is to apply vibrations on the skin layer immediately adjacent to the bone, and measure the response at neighboring locations. Although the signal can be expected to propagate to the bone and subsequently to the inner trabecular bone, due to impedance mismatch there will be reflections at the skin-cortical and cortical-trabecular interfaces. To estimate the response of trabecular bone, it is necessary to be able to differentiate it from these complementary signals. Similar problems arise in using sonic techniques for underwater exploration of petroleum deposits, and recent studies have addressed some of these issues. The solutions involve measurements of responses of a signal from detectors at multiple locations (47). We are currently adapting these methods to develop algorithms to delineate responses of cortical and trabecular segments from that of the whole bone.

The authors thank Michael Marder, Sid Nagel, George Reiter, and Jesper Thomsen for their suggestions.

This work is partially funded by grants from the National Science Foundation and the Institute for Space Science Operations (to G.H.G.).

REFERENCES

1. Gao, H., B. Ji, I. L. Jäger, E. Artz, and P. Fratzl. 2003. Materials become insensitive to flaws at nanoscale: lessons from nature. *Proc. Natl. Acad. Sci. USA*. 100:5597–5600.
2. Ji, B., H. Gao, and K. J. Hsia. 2004. How do slender mineral crystals resist buckling in biological materials? *Philos. Mag. Lett.* 84: 631–641.
3. Blank, R. D. 2001. Breaking down bone strength: a perspective of the future of skeletal genetics. *J. Bone Min. Res.* 16:1207–1211.
4. Bolotin, H. H., and H. Sievänen. 2001. Inaccuracies inherent in dual-energy x-ray absorptiometry in vivo bone mineral density can seriously mislead diagnostic/prognostic interpretation of patient-specific bone fragility. *J. Bone Min. Res.* 16:799–805.
5. Keaveny, T. M., and W. C. Hayes. 1993. A 20-year perspective on the mechanical properties of bone. *Trans. ASME*. 115:534–542.

6. McCreddie, B. R., and S. A. Goldstein. 2000. Biomechanics of fracture: is bone mineral density sufficient to assess risk? *J. Bone Min. Res.* 15:2305–2308.
7. Mosekilde, L., L. Mosekilde, and C. C. Danielsen. 1987. Biomechanical competence of vertebral trabecular bone in relation to ash density and age in normal individuals. *Bone*. 8:79–85.
8. Recker, R. R. 1989. Low bone mass may not be the only cause of skeletal fragility in osteoporosis. *Proc. Soc. Exp. Biol. Med.* 191:272–274.
9. Silva, M. J., and L. J. Gibson. 1997. Modeling the mechanical behavior of vertebral trabecular bone: effects of age-related changes in microstructure. *Bone*. 21:191–199.
10. Silva, M. J., and L. J. Gibson. 1997. The effects of non-periodic microstructure and defects on the compressive strength of two-dimensional cellular solids. *Int. J. Mech. Sci.* 39:549–563.
11. Silva, M. J., W. C. Hayes, and L. J. Gibson. 1995. The effects of non-periodic microstructure of the elastic properties of two-dimensional cellular solids. *Int. J. Mech. Sci.* 37:1161–1177.
12. Guo, X. E., and C. H. Kim. 2002. Mechanical consequences of trabecular bone loss and its treatment: a three-dimensional model simulation. *Bone*. 30:404–411.
13. Stauffer, D. 1985. *Introduction to Percolation Theory*. Taylor and Francis, London.
14. Bell, G. H., O. Dunbar, J. S. Beck, and A. Gibb. 1967. Variations in strength of vertebrae with age and their relation to osteoporosis. *Calcif. Tissue Res.* 1:75–86.
15. Carter, D. R., and W. C. Hayes. 1977. The compressive behavior of bone as a two-phase porous structure. *J. Bone Joint Surg. Am.* 59:954–962.
16. McBroom, R. J., W. C. Hayes, W. T. Edwards, R. P. Goldberg, and A. A. White III. 1985. Prediction of vertebral body compressive fracture using quantitative computed tomography. *J. Bone Joint Surg. Am.* 67:1206–1214.
17. McElhaney, J. H., J. L. Fogle, J. W. Melvin, R. R. Haynes, V. L. Roberts, and N. M. Alem. 1970. Mechanical properties of cranial bone. *J. Biomech.* 3:495–511.
18. Rice, J. C., S. C. Cowin, and J. A. Bowman. 1988. On the dependence of the elasticity and strength of cancellous bone on apparent density. *J. Biomech.* 21:155–168.
19. Mosekilde, L. 1988. Age-related changes in vertebral trabecular bone architecture—assessed by a new method. *Bone*. 9:247–250.
20. Rajapakse, C. S., J. S. Thomsen, J. S. Espinoza Ortiz, S. J. Wimalawansa, E. N. Ebbesen, L. Mosekilde, and G. H. Gunaratne. 2004. An expression relating breaking stress and density of trabecular bone. *J. Biomech.* 37:1241–1249.
21. Espinoza Ortiz, J. S., C. S. Rajapakse, and G. H. Gunaratne. 2002. Strength reduction in electrical and elastic networks. *Phys. Rev. B.* 66:144203-1–144203-8.
22. Gunaratne, G. H. 2002. Estimating the strength of bone using linear response. *Phys. Rev. E. Stat. Nonlin. Soft Matter Phys.* 66:062904-1–062904-5.
23. Song, Y., M. A. K. Liebschner, and G. H. Gunaratne. 2004. Architectural changes of trabecular bone that affect its fracture load. *Biophys. J.* 87:3642–3647.
24. Espinoza Ortiz, J. S., and G. H. Gunaratne. 2002. Current distributions in fused electrical networks. *Braz. J. Phys.* 33:368–375.
25. Harlow, D. G., and S. L. Phoenix. 1981. Probability distributions for the strength of composite materials. II. A convergent sequence of tight bounds. *Intl. J. Fracture*. 17:601–630.
26. Gunaratne, G. H., C. S. Rajapakse, K. E. Bassler, K. K. Mohanty, and S. J. Wimalawansa. 2002. A model for bone strength and osteoporotic fracture. *Phys. Rev. Lett.* 88:068101.
27. Hildebrand, T., A. Laib, R. Müller, J. Dequeker, and P. Rüegsegger. 1999. Direct three-dimensional morphometric analysis of human cancellous bone: microstructural data from spine, femur, iliac crest, and calcaneus. *J. Bone Min. Res.* 7:1167–1174.
28. Rüegsegger, P., B. Koller, and R. Müller. 1996. A microtomographic system for the non-destructive evaluation of bone architecture. *Calcif. Tissue Int.* 58:24–29.
29. Ladd, A. J. C., and J. H. Kinney. 1997. Elastic constants of cellular structures. *Physica A (Amsterdam)*. 240:349–360.
30. Ladd, A. J. C., J. H. Kinney, and T. M. Breunig. 1997. Deformation and failure in cellular materials. *Phys. Rev. E.* 55:3271–3275.
31. Frisch, U., D. d'Humières, B. Hasslacher, P. Lallemand, and Y. Pomeau. 1987. Lattice gas hydrodynamics in two and three dimensions. *Complex Sys.* 1:649–707.
32. Press, W. H., B. P. Flannery, S. A. Teukolsky, and W. T. Vetterling. 1988. *Numerical Recipes—The Art of Scientific Computing*. Cambridge University Press, Cambridge, UK.
33. Ciarelli, T. E., D. P. Fyhrie, M. B. Schaffler, and S. A. Goldstein. 2000. Variations in three-dimensional cancellous bone architecture of the proximal femur in female hip fractures and in controls. *J. Bone Min. Res.* 15:32–40.
34. Hogan, H. A., S. P. Ruhmann, and H. W. Sampson. 2000. The mechanical properties of cancellous bone in the proximal tibia of ovariectomized rats. *J. Bone Min. Res.* 15:284–292.
35. Morgan, E. F., H. H. Bayraktar, O. C. Yeh, S. Majumdar, A. Burghardt, and T. M. Keaveny. 2004. Contribution of inter-site variations in architecture to trabecular bone apparent yield strains. *J. Biomech.* 37:1413–1420.
36. Morgan, E. F., and T. M. Keaveny. 2001. Dependence of yield strain of human trabecular bone on anatomic site. *J. Biomech.* 34:569–577.
37. Niebur, G. L., M. J. Feldstein, J. C. Yuen, and T. M. Keaveny. 2000. High resolution finite element models with tissue strength asymmetry accurately predict failure of trabecular bone. *J. Biomech.* 33:1575–1583.
38. Rho, J. Y., R. B. Ashmas, and C. H. Turner. 1993. Young's modulus of trabecular and cortical bone material: ultrasonic and microtensile measurements. *J. Biomech.* 26:111–119.
39. Ryan, S. D., and J. L. Williams. 1989. Tensile testing of rodlike trabeculae excised from bovine femoral bone. *J. Biomech.* 22:351–355.
40. Bourne, B. B., and M. C. H. van der Meulen. 2004. Finite element models predict cancellous apparent modulus when tissue modulus is scaled from specimen CT-attenuation. *J. Biomech.* 37:613–621.
41. Keaveny, T. M., R. E. Borchers, L. J. Gibson, and W. C. Hayes. 1993. Theoretical analysis of experimental artifact in trabecular bone compressive modulus. *J. Biomech.* 26:599–607.
42. Van der Linden, J. C., J. A. N. Verhaar, and H. Weinans. 2001. A three-dimensional simulation of age-related remodeling in trabecular bone. *J. Bone Min. Res.* 16:688–696.
43. Niebur, G. L., J. C. Yuen, A. C. Hsia, and T. M. Keaveny. 1999. Convergence behavior of high-resolution finite element models of trabecular bone. *J. Biomech. Eng.* 121:629–635.
44. Fischer, K. J., C. R. Jacobs, M. E. Levensen, and D. R. Carter. 1997. Observations of convergence and uniqueness of node-based bone remodeling simulations. *Ann. Biomed. Eng.* 25:261–268.
45. Chakrabarti, B. K., and L. G. Benguigui. 1997. *Statistical Physics of Fracture and Breakdown in Disordered Systems*. Oxford University Press, New York.
46. Chesnut, C. H., and C. J. Rose. 2001. Reconsidering the effects of anti-resorptive therapies in reducing osteoporosis fracture. *J. Bone Miner. Res.* 15:32–40.
47. Weglein, A. B., F. V. Araújo, P. M. Carvalho, R. H. Stolt, K. H. Matson, R. T. Coates, D. Corrigan, D. J. Foster, S. A. Shaw, and H. Zhang. 2003. Inverse scattering series and seismic exploration. *Inverse Problems*. 19:R27–R83.